Satellite structure of the neon valence shell by electron-momentum spectroscopy

O. Samardzic, S. W. Braidwood, E. Weigold,* and M. J. Brunger
Institute for Atomic Studies, School of Physical Sciences, The Flinders University of South Australia, GPO Box 2100, Adelaide, South Australia, 5001, Australia
(Received 15 June 1993)

Momentum distributions and spectroscopic factors are obtained in a high-resolution electron-momentum spectroscopy study of neon at 1500 eV. The shapes and relative magnitudes of the momentum profiles are in good agreement with the results of calculations made within the distorted-wave Born approximation (DWBA) and target Hartree-Fock approximation frameworks. The DWBA accurately describes the relative magnitudes of the $2p$ and $2s$ manifold cross sections as well as the shape of the $2s$ cross section. Results for the momentum profiles belonging to excited $^2P^o$ and $^2S^e$ manifolds are also presented. Spectroscopic factors for transitions belonging to the $^2P^o$ and $^2S^e$ manifolds are assigned up to a binding energy of 95 eV. The spectroscopic factor for the lowest $2s$ transition is 0.85 ± 0.02, whereas that for the ground-state $2p$ transition is 0.92 ± 0.02. Comparison of the present binding energies and spectroscopic factors are made against the results of several many-body calculations and photoelectron-spectroscopy (PES) results. The ramifications of the present work to earlier PES classifications of the correlation satellites are also considered.

PACS number(s): 34.80.Dp, 35.10.Hn

INTRODUCTION

The presence of correlation satellite structures in electron-momentum spectroscopy (EMS) and photoelectron (PE) spectra is still a challenging problem both from the theoretical and the experimental points of view and, although its origin is quite clear [1], there are still many features which are not fully understood. The inner valence region usually exhibits the most intense and complicated structures [2] and therefore provides a wealth of information and a difficult test case for the theoretical models employed in the calculations, which have to take into account properly many-body electron-correlation effects in order to reproduce quantitatively both the binding energies and spectroscopic factors of the satellites. Consequently, EMS and photoelectron spectroscopy (PES) measurements provide information that represents a sensitive and important test of the quality of the theoretical description of the atomic (and molecular) electronic structure.

A particularly fertile area of study has been the valence electronic structure of the rare gases and their ions. Extensive EMS studies of argon (McCarthy *et al.* [3] and references therein) and xenon (Braidwood, Brunger, and Weigold [4] and references therein) and similarly extensive PES studies of neon, argon, krypton, and xenon (Svenson *et al.* [5] and Krause *et al.* [6] and references therein) have been reported in the literature. Much of this work has focused on the ionization of the outer-shell s electrons, as this is a process of particular importance in studying atomic many-electron correlations. It is generally believed [7] that at high energies the observed electron-binding-energy spectrum should not depend on the ionization mechanism. Generally, target ground-state correlations are not important and the binding-energy spectra can be described mainly by many-electron correlations in the final state of the ion. In this approximation relative line intensities in the binding-energy spectra, which are equal to the spectroscopic factors or pole strengths of the corresponding ion states, are determined by the probability of finding the ion in the pure one-hole state [2]. Note that we define the spectroscopic factor $S_j^{(f)}$ as the probability of finding the one-hole configuration j in the expansion of the final ion state and furthermore it satisfies the sum rule [2] $\sum_f S_j^{(f)}=1$. However, inconsistencies exist between PES measurements at different photon energies and between the PES and EMS data [3,4]. Part of this difference in spectroscopic strengths is due to the inherent difficulty in PES of measuring the strength in the continuum [8], whereas there is in principle no difficulty in this for EMS. The accuracy obtained in determining the continuum contribution in EMS depends only on the statistical accuracy of the true and accidental coincidence count rates at the relevant binding energies and on the accuracy of the ratio of the true to accidental window widths [2]. However, the main difference between EMS and PES is that PES probes the high-momentum region of the wave function, the momentum depending on the electron and photon energies. In the high-momentum region ground-state correlations become important. Amusia and Kheifets [9–11] and Kheifets [12], in a series of Green's-function calculations, claim to have shown that these correlations give a contribution to the ionization amplitude that is different for the ground and excited ion states for any symmetry manifold and can potentially change the relative intensities of the main and satellite lines in the binding-energy spectrum. For EMS, where the momentum transferred to the ion is small, these effects are negligible and the relative line intensities correspond to the true spectroscopic factors, i.e., the square of the absolute value of the ion-target overlap function. On the other hand, for the case

of photoionization, where the momentum transferred to the ion is large, these ground-state correlation effects are significant and the resulting PES line intensities can deviate significantly from the standard spectroscopic factors. We note that this interpretation has not been universally accepted by the PES scientific community and so remains controversial. Nevertheless, Amusia and Kheifets [10,11] found quite good agreement with their Green's-function calculations of the spectroscopic factors with EMS data for argon [10] and xenon [11] and they also found that if the spectroscopic factors are corrected by the inclusion of high-momentum components of the ground-state correlation effects, good agreement is obtained with the PES results. Hence they [11] concluded that since PES probes the very-high-momentum part of the many-electron wave function it does not obtain "true" spectroscopic factors. They showed that EMS on the other hand, obtains true spectroscopic factors since it probes the low-momentum region of the wave function, corresponding to the outer region in coordinate space where the electron probability density is high for valence electrons.

Previous EMS investigations into the valence electronic structure of neon have been limited. They include the early study of Dixon *et al.* [13] who successfully implemented a fully partial-wave-expanded distorted-wave approximation to confirm the spectroscopic sum rule, and hence the validity of the structure determination for neon. The energy resolution of this work was rather broad at 3.5 eV full width at half maximum (FWHM) and it did not study correlation satellites in any detail, although they observed a small satellite peak at a binding energy of about 59.5 eV associated with ionization from the $2s$ manifold. Leung and Brion [14] also found some evidence for a small satellite peak at 59.5 eV. More recently, Braidwood *et al.* [15] studied the isoelectronic species hydrogen fluoride and neon. In this work they concentrated on the main $2p^{-1}$ and $2s^{-1}$ lines and, by comparing the measured momentum distributions with the results of their plane-wave and distorted-wave Born approximation (PWBA and DWBA) calculations, they were able to advance a plausible explanation for the observed discrepancy between theory and experiment for the inner-valence 2σ cross section of hydrogen fluoride. Brunger and Weigold [16] reported the first detailed EMS measurement of the satellite structure of the neon valence shell. In this work binding-energy spectra were measured at $\phi=0°$ and 10° over the binding-energy range 18–90 eV and spectroscopic factors were derived. The present study represents a significant extension of this earlier work [16].

From a theoretical perspective Dyall and Larkins [17,18] have applied their frozen-core configuration-interaction (CI) model to calculate the $^2S^e$ and $^2P^o$ satellite structure of neon up to binding energies of about 68 eV. Decleva *et al.* [19], in an increasingly sophisticated series of calculations up to the four-hole–three-particle ($4h$-$3p$) level, performed CI calculations for the lowest satellite states (up to binding energies of about 60 eV) of neon and argon. In this work they studied extensively the effect that improving the treatment of correlation in their model had on the calculated satellite intensities and binding energies. Finally, we note the recent work of Brosolo *et al.* [20] who calculated binding energies and spectroscopic factors for the main $2p^{-1}$ and $2s^{-1}$ lines and who also gave the sum of the remaining pole strengths for the other satellites of the $^2S^e$ and $^2P^o$ manifolds.

In the present work we report an accurate 1500-eV EMS study of the valence electronic structure of neon, up to a binding energy of 95 eV. Spectroscopic factors for transitions belonging to the $^2P^o$ manifolds are assigned and results for the momentum profiles belonging to excited $^2P^o$ and $^2S^e$ manifolds are presented and discussed.

EXPERIMENTAL METHODS

The electron-coincidence spectrometer and the general techniques used in the present measurements have been described in some detail previously [2,7], and so only a

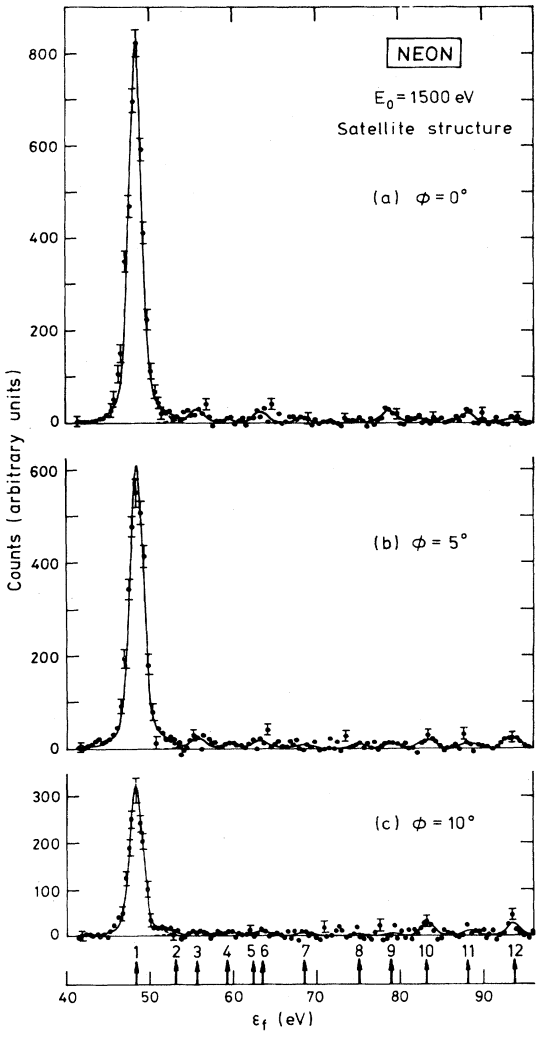

FIG. 1. The 1500-eV noncoplanar symmetric EMS binding-energy spectra at (a) $\phi=0°$, (b) $\phi=5°$, and (c) $\phi=10°$. The curves show the fitted spectra using the known energy-resolution function.

TABLE I. Spectroscopic factors $S_i^{(f)}$ for the main $2p^{-1}$ and $2s^{-1}$ lines and respective sums of the excited $^2P^o$ and $^2S^e$ manifold satellites of neon as a function of the out-of-plane azimuthal angle ϕ. Also shown are the results of the calculations of Dyall and Larkins [17,18] (FCCI) and Brosolo *et al.* [20] ($3h$-$1p$). The one standard deviation error in the last significant figure is given in parentheses.

		$S_i^{(f)}$											
		ϕ (deg)										Theory	
State	Classification	0	1	2	3	5	7	10	15	20	25	FCCI	$3h$-$1p$
Main $2s^{-1}$ line	$2s^1 2p^6$	0.86(1)	0.84(1)	0.85(1)	0.87(2)	0.87(2)	0.85(2)	0.82(3)	0.80(4)	0.82(9)	0.83(10)	0.96	0.86
$\sum$ states 2–9 +state 11		0.14(2)	0.16(2)	0.15(2)	0.13(3)	0.13(3)	0.15(3)	0.18(4)	0.20(5)	0.18(5)	0.17(6)		0.14
Main $2p^{-1}$ line	$2s^2 2p^5$	0.90(3)	0.92(3)	0.87(5)	0.90(2)	0.93(2)	0.92(1)	0.93(1)	0.93(2)	0.95(3)	0.92(4)	0.97	0.93
$\sum$ states 10 and 12		0.10(4)	0.08(4)	0.13(6)	0.10(3)	0.07(3)	0.08(2)	0.07(2)	0.07(3)	0.05(4)	0.08(5)		0.07

brief outline need be given here. The only major recent change to the noncoplanar symmetric coincidence spectrometer has been the inclusion of a differentially pumped collision chamber. The high-purity neon is admitted into the target chamber through a capillary tube, the leak rate being controlled by a Granville-Phillips variable leak valve. The collision region is surrounded by a chamber pumped by a 700-l s^{-1} diffusion pump. Apertures and slits are cut in the collision chamber for the incident beam and ejected electrons. The differentially pumped collision region makes it possible to increase the target-gas density by a factor of about 2 while keeping the background pressure in the spectrometer below 10^{-5} Torr. This allowed us to operate the electron beam at a lower current (typically 80 μA in the present work), resulting in a better energy resolution. The energy resolution of the spectrometer is limited by the energy spread of the incident beam due to space-charge effects [2]. The energy resolution of the present measurements is 1.64 eV (FWHM), and the angular resolution is $\Delta\phi = 1.25°$ (FWHM). These values are degraded slightly compared to those of Brunger and Weigold [16], a situation which was forced upon us to make the measurements of the correlation satellite momentum distributions feasible.

Operating conditions were chosen so that the incident energy $E_0 = 1500$ eV + binding energy (ε_f), the ejected electrons had energies E_A and E_B in the range 750 ± 7 eV and made angles of 45° with respect to the incident-electron direction. The out-of-plane azimuthal angle ϕ was varied over the angular range 0°–25° in order to vary the recoil momentum as

$$p = \left[(2p_A \cos\theta - p_0)^2 + 4p_A^2 \sin^2\theta \sin^2\frac{\phi}{2} \right]^{1/2} . \quad (1)$$

Binding-energy spectra were taken at each out-of-plane azimuthal angle over the range $\varepsilon_f = 18$–95 eV using the binning mode [2].

THEORETICAL BACKGROUND

A thorough description of the DWBA calculations used in the present study can be found elsewhere [15]. Briefly, however, the differential cross section for the ionization of an atom by electron impact, without capture processes, is given by

$$\frac{d^5\sigma_{fi}}{d\Omega_A d\Omega_B dE_A} = \frac{(2\pi)^4}{4} \frac{k_A k_B}{k_0} \times \sum_S (2S+1) |T_{fi}^{(S)}(\mathbf{k}_A, \mathbf{k}_B, \mathbf{k}_0)|^2 , \quad (2)$$

where $\mathbf{k}_0$, $\mathbf{k}_A$, and $\mathbf{k}_B$ are the momenta of the incoming and two outgoing electrons, respectively. The singlet ($S=0$) and triplet ($S=1$) T matrix is given by

$$T_{fi}^{(S)}(\mathbf{k}_A, \mathbf{k}_B, \mathbf{k}_0) = \langle \psi_f^{(-)}(\mathbf{k}_A, \mathbf{k}_B) | V[1 + (-1)^S P_r] | \psi_{i,S}^{(+)}(\mathbf{k}_0) \rangle , \quad (3)$$

where P_r is the space-exchange operator between the incident and ejected electrons. $\psi_{i,S}^{(+)}(\mathbf{k}_0)$ and $\psi_f^{(-)}(\mathbf{k}_A, \mathbf{k}_B)$ are the initial and final total wave functions which are the solutions of the respective Schrödinger equations:

$$(H - E^{(+)})\psi_{i,S}^{(+)}(\mathbf{k}_0) = 0 \quad (4)$$

and

$$(H - V - E^{(-)})\psi_f^{(-)}(\mathbf{k}_A, \mathbf{k}_B) = 0 . \quad (5)$$

Here H is the total Hamiltonian of the system and V is the electron-electron Coulomb interaction between the incident and ejected electrons.

$$V(\mathbf{r}_1, \mathbf{r}_2) = \frac{1}{|\mathbf{r}_1 - \mathbf{r}_2|} , \quad (6)$$

The above formulas for the $(e,2e)$ process include only the direct and exchange scattering, omitting the capture scattering which describes a process by which the incident electron knocks out two target electrons and is captured by the target. It was shown previously [21] that the capture-scattering process becomes negligible at incident-electron energies of 200 eV and higher for the case of electron-impact ionization of helium and therefore this process was omitted in the present calculations.

To calculate $\psi_{i,S}^{(+)}(\mathbf{k}_0)$ and $\psi_f^{(-)}(\mathbf{k}_A, \mathbf{k}_B)$, Braidwood *et al.* [15] use the DWBA:

$$\psi_{i,S}^{(+)}(\mathbf{k}_0,\mathbf{r}_1,\ldots,\mathbf{r}_N)\approx\xi_S^{(+)}(\mathbf{k}_0,\mathbf{r}_1)\Phi_i(\mathbf{r}_2,\ldots,\mathbf{r}_N)\ , \tag{7}$$

$$\psi_f^{(-)}(\mathbf{k}_A,\mathbf{k}_B,r_1,\ldots,\mathbf{r}_N)\approx\chi^{(-)}(\mathbf{k}_A,\mathbf{r}_1)\chi^{(-)}(\mathbf{k}_B,\mathbf{r}_2)\Phi_f(\mathbf{r}_3,\ldots,\mathbf{r}_N)\ , \tag{8}$$

where the ground state of the atom is approximated by the one-configuration Hartree-Fock wave function Φ_i, and the final state of the residual ion is approximated by Φ_f, which is Φ_i with a hole in one of the orbitals, say Φ_j. This final-state approximation is equivalent to taking the sum over all final states belonging to that orbital.

Using the above approximations, the T matrix $T_{fi}^{(S)}(\mathbf{k}_A,\mathbf{k}_B,\mathbf{k}_0)$ [Eq. (3)] becomes

$$T_{fi}^{(S)}(\mathbf{k}_A,\mathbf{k}_B,\mathbf{k}_0)=\langle\chi^{(-)}(\mathbf{k}_A)\chi^{(-)}(\mathbf{k}_B)|V[1+(-1)^S P_r]|\xi_S^{(+)}(\mathbf{k}_0)\phi_j\rangle\ , \tag{9}$$

where ϕ_j is the Hartree-Fock orbital of the knocked-out electron with quantum numbers nlm, $\xi_S^{(+)}(\mathbf{k}_0)$ the distorted wave for the incident electron generated in the static-exchange potential of the atom, and $\chi^{(-)}(\mathbf{k}_A)$, $\chi^{(-)}(\mathbf{k}_B)$ the distorted waves for the electrons moving in the static potential of the residual ion. These wave functions, $\chi^{(-)}(\mathbf{k}_A)$, $\chi^{(-)}(\mathbf{k}_B)$, and $\xi^{(+)}(\mathbf{k}_0)$ are calculated using the partial-wave-expansion formalism via the frozen-core Hartree-Fock program [22]. The ground state Φ_i is calculated using the SCF Hartree-Fock program [23].

In the specific case of electron-impact ionization of neon from the $2s$ and $2p$ shells, we have

$$\frac{d^5\sigma_{2s}}{d\Omega_A d\Omega_B dE_A}=2\frac{(2\pi)^4}{4}\frac{k_A k_B}{k_0}\sum_S(2S+1)|T_{2s}^{(S)}(\mathbf{k}_A,\mathbf{k}_B,\mathbf{k}_0)|^2\ , \tag{10}$$

$$\frac{d^5\sigma_{2p}}{d\Omega_A d\Omega_B dE_A}=2\frac{(2\pi)^4}{4}\frac{k_A k_B}{k_0}\sum_{m,S}(2S+1)|T_{2p,m}^{(S)}(\mathbf{k}_A,\mathbf{k}_B,\mathbf{k}_0)|^2\ . \tag{11}$$

Note that the present DWBA momentum distributions are all folded with the experimental angular resolution for comparison with the experimental data.

RESULTS AND DISCUSSION

Binding-energy spectrum

The binding-energy spectrum of neon in the region $\varepsilon_f\sim 42-95$ eV is shown in Fig. 1 for a total energy of 1500 eV and with the out-of-plane azimuthal angles $\phi=0°$, $\phi=5°$, and $\phi=10°$. At $\phi=0°$, the momentum p ranges from 0.245 a.u. at the binding energy of the first peak ($\varepsilon_f=48.46$ eV) to 0.366 a.u. for $\varepsilon_f=93.61$ eV. At $\phi=5°$, the corresponding momenta are 0.516 and 0.585 a.u., respectively, while at $\phi=10°$, the relevant momenta are 0.945 and 0.985 a.u., respectively. The spectra in Fig. 1 reproduce all the correlation satellites found by Brunger and Weigold [16], and an additional satellite at $\varepsilon_f=93.61$ eV.

For the sake of clarity the $2p^{-1}$ ($2s^2 2p^5$) ground-state transition is not included in the spectra. At $\phi=0°$, i.e., at low momenta, the $2p$ ground-state cross section is only 16% of that for the main $2s^{-1}$ transition ($2s^1 2p^6$) at 48.46 eV, whereas at $\phi=10°$, its cross section is about two-and-one-half times that of the 48.46-eV transition. Thus any reasonable excited $^2P^o$ manifold satellite intensity in the range $\varepsilon_f=42-95$ eV should be noticeable in Fig. 1 by peaks which are much stronger in intensity at $\phi=10°$ than at $\phi=0°$. Peaks 10 and 12, with respective centroid binding energies of 83.34 and 93.61 eV, are obviously such a case. On the other hand, transitions belonging to excited $^2S^e$ manifold satellites should have a much larger intensity at $\phi=0°$ compared to $\phi=10°$. Peaks 1–9 and peak 11 of Fig. 1 clearly correspond to this behavior.

In Table I we present the dependence of the spectroscopic factors $S_i^{(f)}$ for the main $2p^{-1}$ and $2s^{-1}$ transitions and the respective sums of $S_i^{(f)}$ for the identifiable (see Fig. 1) excited $^2P^o$ and $^2S^e$ manifold satellites on the out-of-plane azimuthal angle ϕ [or from Eq. (1), the momentum p]. Also included in this table are the corresponding results for $S_i^{(f)}$ from the frozen-core configuration-interaction (FCCI) calculation of Dyall and Larkins [17,18] and the recent, three-hole–one-particle ($3h$-$1p$) configuration-interaction calculation, of Brosolo *et al.* [20]. It is immediately apparent from Table I that within the stated uncertainties on the present data, the spectroscopic factors of the correlation satellites for both the $^2P^o$ and $^2S^e$ manifolds are independent of the target-electron momentum. Furthermore, on comparison with the results for $S_i^{(f)}$ of Brosolo *et al.* [20] we see that the level of agreement between this theory and the present experiment is good.

We note that the spectroscopic factors for final states belonging to the $2s$ and $2p$ manifolds can in principle be obtained from the momentum profiles to be discussed in the next subsection or, as we did for Table I, from the relative intensities obtained from the energy spectra (see Fig. 1). The results from either technique were found to be consistent for the present study and they are presented in Table II along with two recent (γ,e) results [5,6] and a recent theoretical calculation [19]. Also included in this table are our assignments of the configurations for transitions 1–12 of Fig. 1 and their respective centroid binding energies.

In attempting to assign configurations for transitions 1–6 of Table II, we made use of the calculations of Dyall and Larkins [17,18] and Decleva *et al.* [19] and the optical data of Persson [24]. Each of these transitions (see Fig. 1) clearly belongs to the ^2S manifold and from Dyall and Larkins [17] and Heinemann *et al.* [25] it is apparent that state 1 has the dominant configuration $2s^1 2p^6\,^2S^e$ and state 2 has the configuration $2s^2 2p^4(^3P)3p\ ^2S^e$, while

states 3–6 belong to either of the respective Rydberg series of final ion states with configurations

$$2s^2 2p^4(^1S)(3,4,\ldots)s\ ^2S^e$$

or

$$2s^2 2p^4(^1D)(3,4,\ldots)d\ ^2S^e\ .$$

Note that in the present work the energy resolution did not allow us to resolve completely states 5 and 6 and thus uniquely determine their spectroscopic factors. Consequently, they are presented as a combined value in Table II. In general, we find largely excellent agreement between the present classification of states 1–6 and those previously put forward by Svensson *et al.* [5]. The only exception to this is for the correlation state at $\varepsilon_f = 53.08$ eV (state 2), which they assigned as being the first member of the

$$2s^2 2p^4(^3P)(3,4,\ldots)p\ ^2P^o$$

series. The present measurements conclusively demonstrate that this state belongs to the $2s$ manifold. We note that although we do not observe the expected

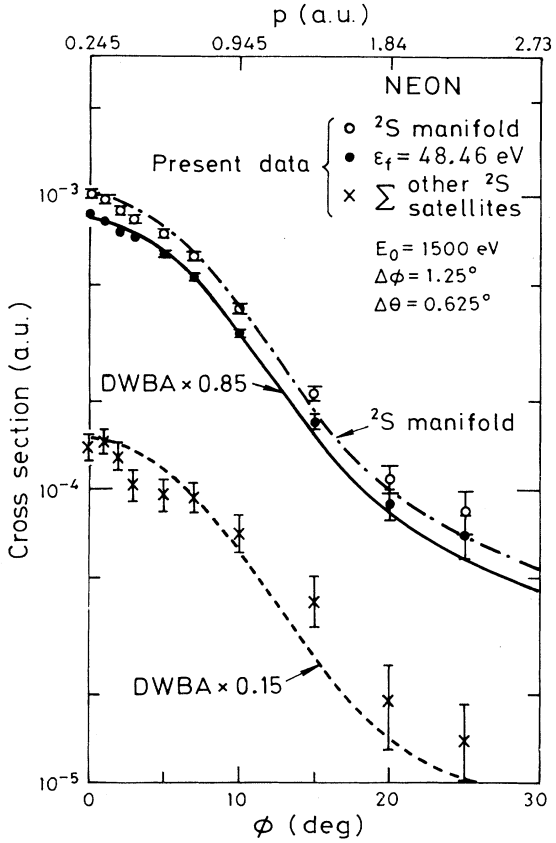

FIG. 2. The 1500-eV noncoplanar symmetric momentum profiles for the total $^2S^e$ manifold (○), the main $2s^{-1}$ line at 48.46 eV (●) and the $\sum$ over all other $2s$ correlation satellites (×), compared with the result of the DWBA (——). All data have been normalized by fitting the measured ground-state transition at $\phi = 10°$ to 0.92 times the $2p$ DWBA cross section.

TABLE II. Comparison of spectroscopic factors for ion states belonging to the $2p$ and $2s$ manifolds of neon. The error in the last significant figure is given in parentheses.

No.	Present EMS			(γ,e)				Theory [19]		
Peak	Main configuration	ε_f (eV)	S_f	Main configuration	$\varepsilon_f^{(a)}$ (eV)	$S_f^{(a)}$	$S_f^{(b)}$	Main configuration	ε_f (eV)	S_f
	$2s^2 2p^5$ $^2P^o$	21.57	0.92(2)	$2s^2 2p^5$ $^2P^o$	21.57	0.99		$2s^2 2p^5$ $^2P^o$	21.58	0.92
1	$2s^1 2p^6$ $^2S^e$	48.46	0.85(2)	$2s^1 2p^6$ $^2S^e$	48.46	0.92	0.82	$2s^1 2p^6$ $^2S^e$	48.52	0.86
2	$2s^2 2p^4(^3P)3p$ $^2S^e$	53.08	0.013(3)	$2s^2 2p^4(^3P)3p$ $^2P^o$	53.08	0.005		$2s^2 2p^4(^3P)3p$ $^2S^e$	52.61	0.002
3	$2s^2 2p^4(^1S)3s$ $^2S^e$	55.83	0.028(8)	$2s^2 2p^4(^1S)3s$ $^2S^e$	55.83	0.022	0.15	$2s^2 2p^4(^1S)3s$ $^2S^e$	55.51	0.016
4	$2s^2 2p^4(^1D)3d$ $^2S^e$	59.49	0.014(3)	$2s^2 2p^4(^1D)3d$ $^2S^e$	59.49	0.009	0.03	$2s^2 2p^4(^1D)3d$ $^2S^e$	59.20	0.010
5	$2s^2 2p^4(^1D)4d$ $^2S^e$	62.19	0.025(6)	$2s^2 2p^4(^1D)4d$ $^2S^e$	62.19	0.002		$2s^2 2p^4(^1D)4d$ $^2S^e$	62.27	0.003
6	$2s^2 2p^4(^1S)4s$ $^2S^e$	63.56		$2s^2 2p^4(^1S)4s$ $^2S^e$	63.56	0.002				
	$2s^2 2p^4(^1D)5d$ $^2S^e$			$2s^2 2p^4(^1D)5d$ $^2S^e$						
7		68.70	0.014(3)		68.20	0.001				
8		75.11	0.011(3)	$2s2p^5(^3P)3s$ $^2P^o$	75.11	0.005				
9		78.90	0.022(4)	$2s2p^5(^3P)3p$ $^2S^e$	78.90	0.012				
10		83.34	0.04(2)	$2s2p^5(^3P)4p$ $^2S^e$	83.34	0.001				
11		88.32	0.023(4)	$2s2p^5(^1P)3p$ $^2S^e$	88.32	0.029				
12		93.61	0.04(2)	$2s2p^5(^1P)4p$ $^2S^e$	93.61	0.004				

[a]Reference [5] ($E_\gamma = 1487$ eV).
[b]Reference [6] ($E_\gamma = 127.45$ eV).

$2s^2 2p^4(^1S)5s,6s$ lines at $\varepsilon_f = 66.2$ and 67.2 eV, respectively, this can be understood in terms of the CI calculations of Dyall and Larkins [18], which showed that the intensities of these $2s^2 2p^4(^1S)5s,6s$ satellites are expected to be very small. In the absence of theory or optical data, we have not attempted to classify states 7–12 of Fig. 1. However, we note that the classification of Svensson *et al.* [5] for states 9 and 11, at $\varepsilon_f = 78.90$ and 88.32 eV, respectively, as being the singlet-triplet pair of configuration $2s2p^5(^{3,1}P)3p\ ^2S^e$ is consistent with our results and indeed there is even a fair correspondence in the spectroscopic factors for these respective transitions as determined by both the EMS and PES techniques. On the other hand they [5] have allocated states 10 and 12 to the 2*s* manifold, whereas the present result conclusively demonstrates that they are excited configurations of the 2*p* manifold, and, similarly, they have assigned state 8 to the 2*p* manifold when it is clearly shown by the present measurements that this state belongs to the 2*s* manifold. As yet, there has not been a classification assigned to state 7 at $\varepsilon_f = 68.70$ eV but it is possible that it may be one of the higher-order members of either of the Rydberg series of final ion states with configurations $2s^2 2p^4(^1S)ns\ ^2S^e$ or $2s^2 2p^4(^1D)nd\ ^2S^e$ with $n > 6$.

On comparing the present EMS spectroscopic factors with the 4*h*-3*p* theory of Decleva *et al.* [19] (see Table II), we find that there is good agreement between the experimental and calculated values for the main $2p^{-1}$ line at $\varepsilon_f = 21.57$ eV and the main $2s^{-1}$ line at $\varepsilon_f = 48.46$ eV. Similarly, there is good agreement for the measured and calculated [19] binding energies of these states. With respect to the lower-lying excited $^2S^e$ manifold states (transitions 2–5) we would characterize the agreement between the present experiment and the calculation [19], within the quoted uncertainties on the experimental $S_i^{(f)}$, as being fair for states 3 and 4 and poor for state 2. As we could not completely resolve states 5 and 6, and have thus combined their measured spectroscopic factors, we cannot directly compare the present result with that calculated by Decleva *et al.* [19] for state 5.

The PES results quoted in Table II were found to depend strongly on E_γ. This is similar to our previous observations in argon [3] and xenon [4] and suggests that neon might also be a fruitful system for the model of Amusia and Kheifets. Finally, we note that the present determination of the spectroscopic factors for the $^2S^e$ and $^2P^o$ manifolds of neon are consistent with that determined previously by Brunger and Weigold [16], particularly when one allows for the fact that the earlier work did not extend its range of measurement of the binding-energy spectra to include the important 2*p* satellite at $\varepsilon_f = 93.61$ eV.

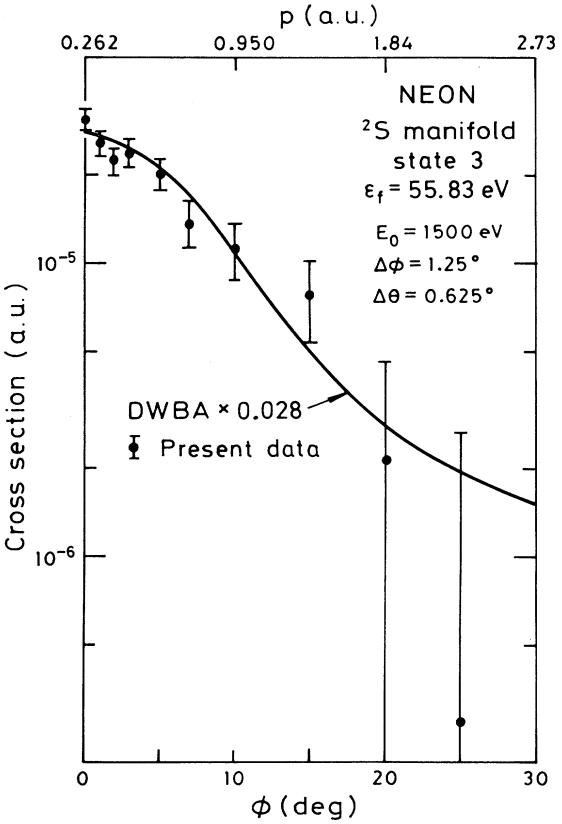

FIG. 3. Momentum profile for the $2s^2 2p^4(^1S)3s\ ^2S^e$ correlation satellite (●) compared with the calculated 2*s* DWBA profile multiplied by 0.028 (——).

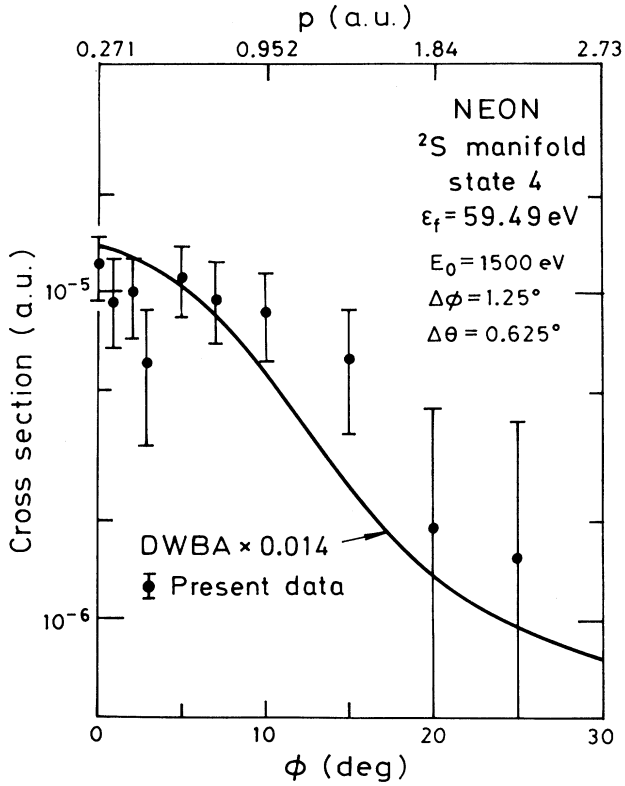

FIG. 4. Momentum profile for the $2s^2 2p^4(^1D)3d\ ^2S^e$ correlation satellite (●) compared with the calculated 2*s* DWBA profile multiplied by 0.014 (——).

Momentum distributions

Binding-energy spectra similar to those shown in Fig. 1 were taken at a range of azimuthal angles. The energy range at each angle and the angular range itself were stepped through repeatedly. Each part of each spectrum at every angle was scanned sequentially for an equal time, each run consisting of many scans. The spectra were then used to obtain cross sections to selected final ion states relative to each other as a function of ϕ or momentum p [Eq. (1)]. In some cases neighboring final ion states could not be completely resolved; where this occurred, they were then grouped under single peaks.

The measured angular correlations (or momentum profiles) are not absolute, but relative normalizations are maintained. The present momentum profiles are normalized to the DWBA by equating the measured intensity at $\phi=10°$ ($p=0.92$ a.u.) in the $2p$ ground-state transition to the DWBA at that point. The DWBA calculations were similar to those reported in the work of Braidwood *et al.* [15]. Nearly all of the $2p$ strength goes to the ground-state transition. This can be seen from Table II. In the present measurements we find the spectroscopic factor for the ground-state transition to be 0.92 ± 0.02, and we have taken this into account in the normalization of the current data.

Figure 2 shows that the DWBA cross section for the $2s$ manifold (open circles) is, within the statistical uncertainties on the measurement, in very good agreement with the measured $2s$ manifold cross section both in shape and in magnitude over the whole angular range of the present experiment. This shows that essentially all of the $2s$ strength has been observed in the measurement over the range $\varepsilon_f=42-95$ eV. Nearly all the strength in this region belongs to the $2s$ manifold; the small $2p$ strengths which are observed and discussed later are not included in the $2s$ manifold cross section shown in the Figure. We note that we do not show the results of our plane-wave Born approximation calculation for the $2s$ manifold of neon in Fig. 2. From a formalism point of view, the PWBA is simply arrived at by replacing the distorted waves $\chi^{(\pm)}(\mathbf{k})$ and $\xi_S^{(+)}(\mathbf{k})$ by plane waves $|\mathbf{k}\rangle$ in Eqs. (9) and (10), respectively. The result of our PWBA calculation was in poor agreement [15] with the present $2s$ manifold measurement (and ipso facto the DWBA) in terms of both the shape and the magnitude of the cross section. In particular, when compared to the present data and the DWBA, the PWBA cross section was found to be too large in magnitude at momenta $p\leq1.65$ a.u. and too small thereafter and, consequently, it is not reproduced in Fig. 2.

The shape of the 48.46-eV transition is virtually indistinguishable from the $2s$ manifold cross section. It is also in good agreement with the DWBA calculation when the calculated $2s$ manifold cross section is multiplied by a factor 0.85 (Fig. 2). Thus, as given in Table II, the spec-

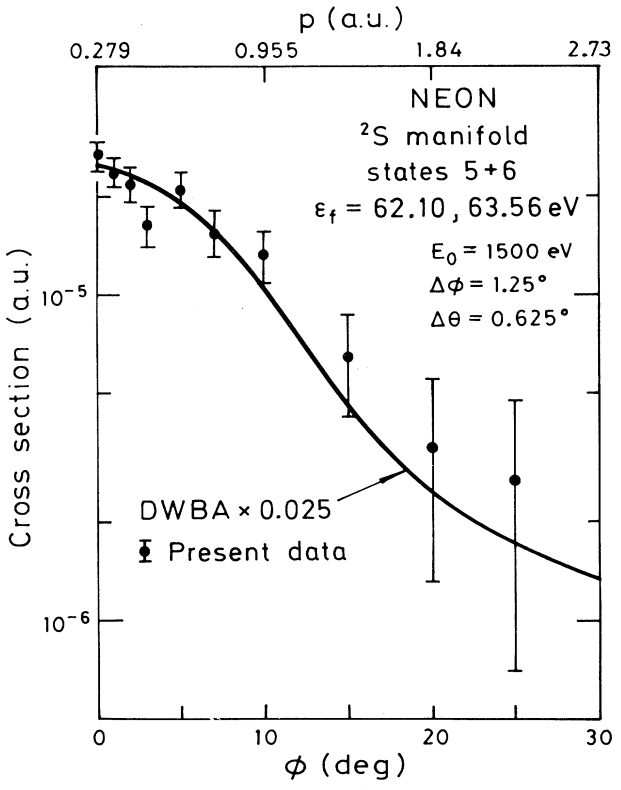

FIG. 5. Momentum profile for the summed $2s^22p^4(^1D)4d\ ^2S^e$ correlation satellite at $\varepsilon_f=62.10$ eV and the $2s^22p^4(^1S)4s\ ^2S^e$ and $2s^22p^4(^1D)5d\ ^2S^e$ satellites at $\varepsilon_f=63.56$ eV (●) compared with the calculated $2s$ DWBA profile multiplied by 0.025 (——).

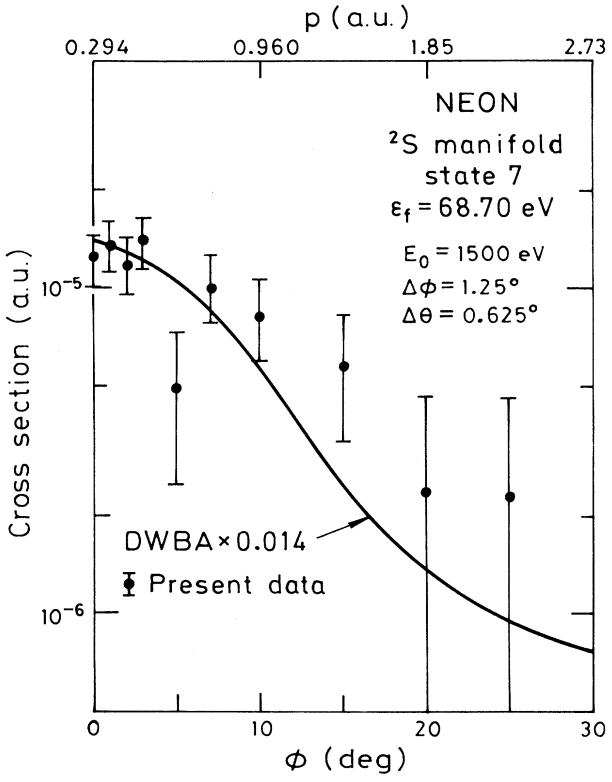

FIG. 6. Momentum profile for the correlation satellite (●) at $\varepsilon_f=68.70$ eV compared with the calculated $2s$ DWBA profile multiplied by 0.014 (——).

troscopic factor for this transition is 0.85, and so the 48.46-eV state, with a dominant configuration of $2s^1 2p^6$, contains about 85% of the $2s$ pole strength.

Figure 2 also shows the momentum profile for the summed cross sections, at each ϕ, of the remaining $2s$ manifold correlation satellites. It is immediately apparent that the shape of this profile, within experimental error, is almost identical to that for the $2s$ manifold and the 48.46-eV transition. Furthermore, this angular correlation is found to be in fair agreement with the DWBA calculation when the theoretical $2s$ manifold cross section is multiplied by a factor of 0.15, a result which is in good agreement with that predicted by the CI calculation of Brosolo *et al.* [20].

In Fig. 3 we show the momentum profile for the $\varepsilon_f = 55.83$ eV $2s^2 2p^4(^1S)3s\ ^2S^e$ satellite (peak 3 of Fig. 1). Again, there is quite good agreement for the shape of this transition and that of the $2s$ manifold. Also, it is in fair agreement with the DWBA calculation when the calculated $2s$ manifold cross section is multiplied by a factor of 0.028. We note that the only exception to this is at $\phi = 25°$ although even here theory and experiment overlap when the uncertainty in the experimental data is taken into account. In principle, the 55.83-eV satellite could also include a transition [6,19] to the odd-parity state $2s^2 2p^4(^1D)3p\ ^2P^o$ at 55.84 eV. However, the excellence of the fit of the present momentum distribution at 55.83 eV to the $2s^{-1}$ DWBA calculation suggests that any con-

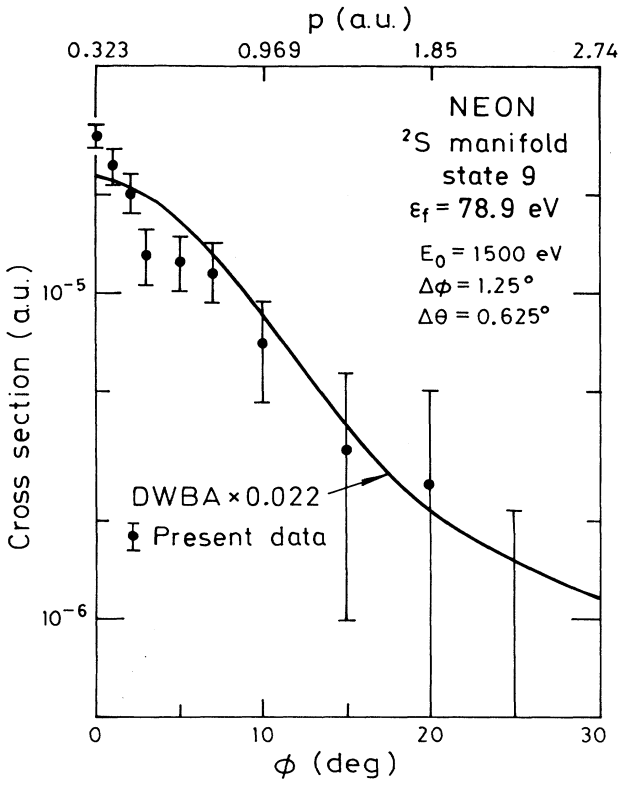

FIG. 8. Momentum profile for the correlation satellite (●) at $\varepsilon_f = 78.90$ eV compared with the calculated $2s$ DWBA profile multiplied by 0.022 (——).

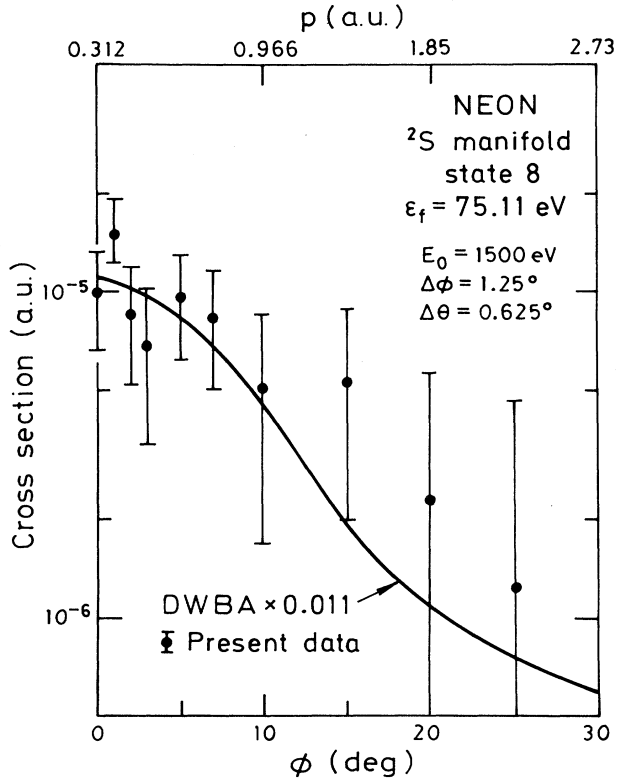

FIG. 7. Momentum profile for the correlation satellite (●) at $\varepsilon_f = 75.11$ eV compared with the calculated $2s$ DWBA profile multiplied by 0.011 (——).

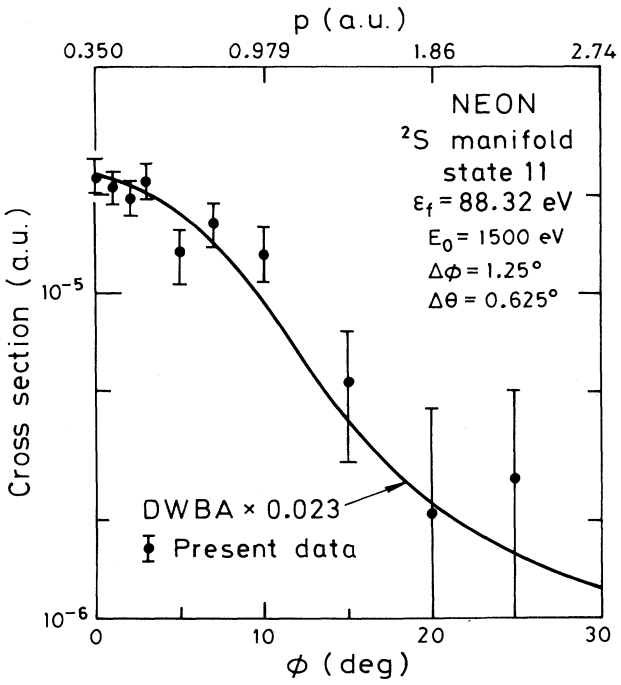

FIG. 9. Momentum profile for the correlation satellite (●) at $\varepsilon_f = 88.32$ eV compared with the calculated $2s$ DWBA profile multiplied by 0.023 (——).

tribution of the odd-parity state must be small. This latter observation is consistent with the calculation of Decleva *et al.* [19] who found that the $2s^2 2p^4(^1D)3p\ ^2P^o$ transition was about four times smaller than the dominant $2s^2 2p^4(^1S)3s\ ^2S^e$ transition.

Figure 4 gives the momentum profile for the $\varepsilon_f = 59.49$ eV, $2s^2 2p^4(^1D)3d\ ^2S^e$ satellite (peak 4 of Fig. 1). The shape of the 59.49-eV transition is, within the experimental error, essentially indistinguishable from the $2s$ manifold cross section and, on comparison with the DWBA calculation, which has been scaled by a factor of 0.014, the level of agreement for the magnitude of the cross section between the present data and theory is also quite good, except at $\phi = 3°$. In this case it is possible for the odd-parity $2s^2 2p^4(^1S)3p\ ^2P^o$ state [6,19] at $\varepsilon_f = 59.38$ eV to contribute to the observed flux. However, the sophisticated calculation of Decleva *et al.* [19] found that the $2s^2 2p^4(^1S)3p\ ^2P^o$ state is 14 times less intense than the dominant $2s^2 2p^4(^1D)3d\ ^2S^e$ line. Also, there is no definitive evidence for a "*p*-like" contribution to our measured angular correlation at 59.49 eV and so we can only conclude that if the $2s^2 2p^4(^1S)3p\ ^2P^o$ configuration is making a contribution to the observed flux at $\varepsilon_f = 59.49$ eV, then it must be a very small contribution.

As discussed previously, the energy resolution of the present study did not permit us to resolve completely states 5 and 6 from each other and so in Fig. 5 we present the summed momentum profile for these transitions. In this case there are no odd-parity states [6] which can contribute to the $2s^2 2p^4(^1D)4d\ ^2S^e$ configuration at $\varepsilon_f = 62.10$ eV and, similarly, there are no odd-parity states which can contribute to the $2s^2 2p^4(^1S)4s\ ^2S^e$ and $2s^2 2p^4(^1D)5d\ ^2S^e$ satellites at $\varepsilon_f = 63.56$ eV. This is well reflected in the good agreement (except at $\phi = 3°$) between the present angular correlation measurement for these states and the result of the DWBA calculation for the $^2S^e$ manifold when the latter is scaled by a factor of 0.025.

The momentum profile for peak 7 of Fig. 1 is given in Fig. 6. To the best of our knowledge, no classification for this state has been provided in the literature [5,6,16] although it is clear from the present angular correlation that it must belong to the $^2S^e$ manifold. Agreement with the DWBA calculation is again fair (except at $\phi = 5°$) when the DWBA is scaled by a factor of 0.014. This is a significant intensity for this satellite when compared to that found in the PES measurement of Svensson *et al.* [5] at $E_\gamma = 1487$ eV ($\sim 0.01\%$).

In Figs. 7, 8, and 9 we illustrate the present momentum distributions for the respective correlation satellites at $\varepsilon_f = 75.11$, 78.90, and 88.32 eV, respectively. In each case the agreement between the present data and the appropriately scaled DWBA calculation is quite good. The present momentum profiles for peaks 9 and 11 at $\varepsilon_f = 78.90$ and 88.32 eV are clearly "*s*-like" and thus belong to the $2s$ manifold. This observation provides supporting evidence for the classification of these transitions

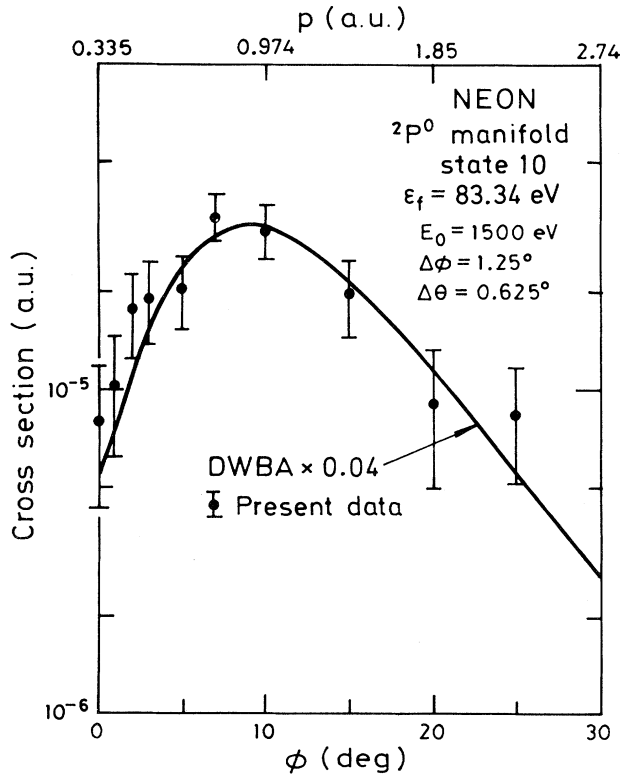

FIG. 10. Momentum profile for the correlation satellite (●) at $\varepsilon_f = 83.34$ eV compared with the calculated $2p$ DWBA profile multiplied by 0.04 (——).

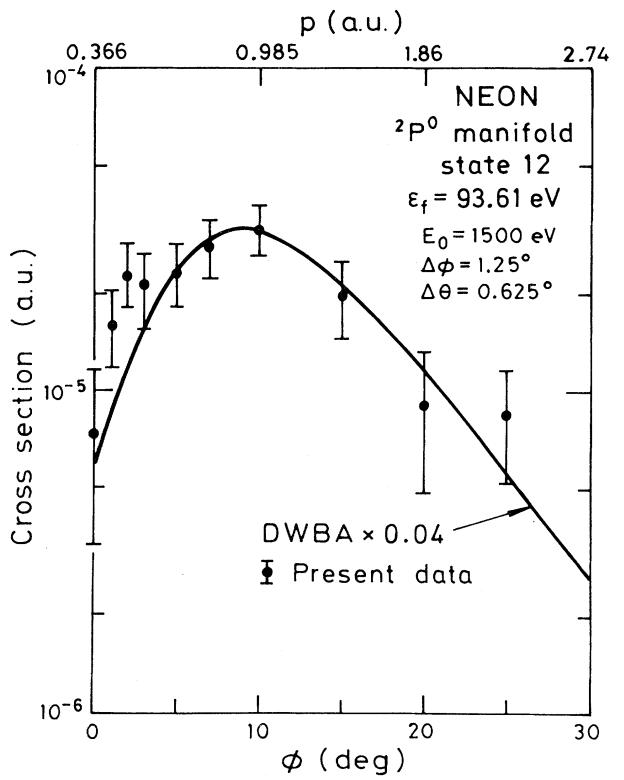

FIG. 11. Momentum profile for the correlation satellite (●) at $\varepsilon_f = 93.61$ eV compared with the calculated $2p$ DWBA profile multiplied by 0.04 (——).

by Svensson *et al.* [5], as being the triplet-singlet pair of states with configuration $2s2p^5(^{3,1}P)3p\ ^2S^e$.

We now turn to transitions which do not belong to the $2s$ manifold. Figures 10 and 11 show the momentum profiles for the 83.34 and 93.61-eV transitions. Their shape is quite different from that for the $2s$ transitions and therefore they cannot belong to the $2s$ manifold. In fact, they are correlation satellites of the $2p$ manifold and Figs. 10 and 11 clearly show that the calculated DWBA $2p$ momentum distribution gives a good fit to each respective angular correlation both in shape and in magnitude, when the DWBA is multiplied by a factor of 0.04. We note that these transitions in the past have been mistakenly assigned to the $2s$ manifold in PES work [5]. In the region from $\varepsilon_f = 75-95$ eV there are several final states that are possible candidates to describe these odd-parity $^2P^o$ satellites. In particular, it is possible that these lines are members of the Rydberg series of configurations $2s2p^5(^{3,1}P)ns\ ^2P^o$ for $n \geq 3$. However, without more supporting optical [24] and theoretical data, any attempt on our part to classify definitively the respective configurations for these transitions would be purely speculative.

CONCLUSIONS

Accurate EMS measurements at 1500 eV have been made for transitions to excited states of Ne^+. The momentum profiles and cross sections relative to the ground-state $2p^{-1}$ transition are accurately described by the distorted-wave Born approximation. Detailed spectroscopic-factor determinations have been obtained for the $2p$ and $2s$ manifolds. The main $2s$ transition at $\varepsilon_f = 48.46$ eV has a spectroscopic strength of 0.85. This is in good agreement with the respective most recent $4h$-$3p$ and $3h$-$1p$ configuration-interaction scheme calculations of Decleva *et al.* [19] and Brosolo *et al.* [20]. Spectroscopic factors for the $2s$ manifold are correctly determined by comparing cross sections for states within the manifold, the sum of the different $2s$ components giving the correct $2s$ manifold cross section normalized relative to the $2p$ cross section. The PES data obtain spectroscopic factors that are somewhat different than those obtained in EMS. At low energies the PES relative intensities are sensitive functions of the energies and depend on the reaction dynamics. At high energies they also probe the high-momentum regions of the target-state correlation effects. As Amusia and Kheifets have proposed, it is necessary to correct these high-recoil-momentum "spectroscopic factors" to obtain true spectroscopic factors. Thus comparison between EMS and PES or structure calculations with PES spectroscopic strength is not always straightforward.

The present measurements reveal important $2p$ strength at higher binding energies in the binding-energy spectrum. They confirm that the $2p^{-1}$ ground-state transition is almost a pure one-hole transition with a spectroscopic factor of 0.92 ± 0.02. This is further verified in the detailed calculations of Decleva *et al.* [19] and Brosolo *et al.* [20].

ACKNOWLEDGMENTS

We are grateful to the Australian Research Council for financial support of this work. Two of us (M.J.B.) and (S.W.B.) also acknowledge the ARC for additional support.

*Permanent address: Research School of Physical Sciences and Engineering, Australian National University, GPO Box 4, Canberra, ACT 2601, Australia.

[1] L. S. Cederbaum, W. Domcke, J. Schirmer, and W. von Niessen, Adv. Chem. Phys. **65**, 115 (1986).
[2] I. E. McCarthy and E. Weigold, Rep. Prog. Phys. **54**, 789 (1991).
[3] I. E. McCarthy, R. Pascual, P. Storer, and E. Weigold, Phys. Rev. A **40**, 3041 (1989).
[4] S. W. Braidwood, M. J. Brunger, and E. Weigold, Phys. Rev. A **47**, 2927 (1993).
[5] S. Svensson, B. Erikson, N. Martensson, G. Wendin, and U. Gelius, J. Electron Spectrosc. Relat. Phenom. **47**, 327 (1988).
[6] M. O. Krause, S. B. Whitfield, C. D. Caldwell, J.-Z. Wu, P. van der Meulen, C. A. de Lange, and R. W. C. Hansen, J. Electron Spectrosc. Relat. Phenom. **58**, 79 (1992).
[7] I. E. McCarthy and E. Weigold, Rep. Prog. Phys. **51**, 299 (1988).
[8] J. D. Mitroy, I. E. McCarthy, and E. Weigold, J. Phys. B **18**, L91 (1985).
[9] M. Ya. Amusia and A. S. Kheifets, J. Phys. B **18**, L679 (1985).
[10] M. Ya. Amusia and A. S. Kheifets, Aust. J. Phys. **44**, 293 (1991).
[11] M. Ya. Amusia and A. S. Kheifets, Phys. Rev. A **46**, 1261 (1992).
[12] A. S. Kheifets, Zh. Eksp. Teor. Fiz. **89**, 459 (1985) [JETP **62**, 260, 1985)].
[13] A. J. Dixon, I. E. McCarthy, C. J. Noble, and E. Weigold Phys. Rev. A **17**, 597 (1978).
[14] K. T. Leung and C. E. Brion, Chem. Phys. **82**, 87 (1983).
[15] S. W. Braidwood, M. J. Brunger, D. A. Konovalov, and E. Weigold, J. Phys. B **26**, 1655 (1993).
[16] M. J. Brunger and E. Weigold, J. Phys. B **25**, L481 (1992).
[17] K. G. Dyall and F. P. Larkins, J. Phys. B **15**, 203 (1982).
[18] K. G. Dyall and F. P. Larkins, J. Phys. B **15**, 229 (1982).
[19] P. Decleva, G. DeAlti, G. Fronzoni, and A. Lisini, J. Phys. B **23**, 3777 (1990).
[20] M. Brosolo, P. Decleva, G. Fronzoni, and A. Lisini, J. Mol. Struct. (to be published).
[21] D. A. Konovalov and I. E. McCarthy (unpublished).
[22] L. V. Chernysheva, N. A. Cherepkov, and V. Radojevic, Comput. Phys. Commun. **11**, 57 (1976).
[23] L. V. Chernysheva, N. A. Cherepkov, and V. Radojevic, Comput. Phys. Commun. **18**, 87 (1979).
[24] W. Persson, Phys. Scr. **3**, 133 (1971).
[25] P. A. Heinemann, U. Becker, H. G. Kerkhoff, B. Langer, D. Szostak, R. Wehiltz, D. W. Lindle, T. A. Ferret, and D. A. Shirley, Phys. Rev. A **34**, 3782 (1986).